https://doi.org/10.5194/cp-2020-46
Preprint. Discussion started: 27 March 2020

Climate of the Past Discussions
Open Access
EGU

Simulating Marine Isotope Stage 7 with a coupled climate-ice sheet model

Dipayan Choudhury[1,2], Axel Timmermann[1,2], Fabian Schloesser[3], Malte Heinemann[4] and David Pollard[5]

[1]Center for Climate Physics, Institute for Basic Science (IBS), Busan 46241, South Korea
[2]Pusan National University, Busan 46241, South Korea
[3]International Pacific Research Center, University of Hawaii at Manoa, Honolulu, HI 96822, USA
[4]Institute of Geosciences, Kiel University, 24118, Kiel, Germany
[5]Earth and Environmental Systems Institute, Pennsylvania State University, Pennsylvania 16802, USA

Correspondence to: Dipayan Choudhury (dipayanc@pusan.ac.kr)

Abstract. It is widely accepted that orbital variations are responsible for the generation of glacial cycles during the late Pleistocene. However, the relative contributions of the orbital forcing compared to CO_2 variations and other feedback mechanisms causing the waxing and waning of ice-sheets have not been fully understood. Testing theories of ice-ages beyond statistical inferences, requires numerical modeling experiments that capture key features of glacial transitions. Here, we focus on the glacial build-up from Marine Isotope Stage (MIS) 7 to 6 covering the period from 240-170 ka (thousand years before present). This transition from interglacial to glacial conditions includes one of the fastest Pleistocene glaciation/deglaciation events which occurred during MIS 7e-7d-7c (236-218ka). Using a newly developed three-dimensional coupled atmosphere-ocean-vegetation-ice-sheet model (LOVECLIP), we simulate the transient evolution of northern and southern hemisphere ice-sheets during the MIS 7-6 period in response to orbital and greenhouse-gas forcing. For a range of model parameters, the simulations capture the reconstructed evolution of global ice volume reasonably well. It is demonstrated that glacial inceptions are more sensitive to orbital variations, whereas terminations from deep glacial conditions need both orbital and greenhouse gas forcings to work in unison. For some parameter values, the coupled model also exhibits a critical North American ice sheet configuration, beyond which a stationary wave – ice-sheet topography feedback can trigger an unabated and unrealistic ice-sheet growth. The strong parameter sensitivity found in this study originates from the fact that delicate mass imbalances, as well as errors, are integrated during a transient simulation for thousands of years. This poses a general challenge for transient coupled climate-ice sheet modeling.

https://doi.org/10.5194/cp-2020-46
Preprint. Discussion started: 27 March 2020

Climate of the Past Discussions
Open Access
EGU

1 Introduction

Earth's climate over the past one million years (Late Quaternary) is characterized by glacial/interglacial cycles representing cold/warm periods, transitioning in timescales of around 80,000-120,000 years. These transitions correspond to global sea level changes of up to 130m (Fig. 1b) (Waelbroeck et al., 2002;Lisiecki and Raymo, 2005;Bintanja et al., 2005). Simulating these massive reorganizations of earth's climate using earth system models of varying complexity is an active area of research. By comparing such simulations with paleoclimate data, we can evaluate the fidelity of these climate models, as well as refine our understanding of the underlying sensitivities and feedbacks to a variety of forcings. One of the main obstacles in simulating variability on orbital timescales is the fact that ice-sheets are slow integrators of small imbalances between ablation and accumulation, which correspond to about 1.3 mm/year global sea level equivalent during the build-up phase. In order to simulate an entire glacial/interglacial cycle, model errors can accumulate for thousands of years and potential multiple equilibria of the fully coupled system can create further complications. Simulating a transient climate "trajectory" realistically is an even bigger modeling and computational challenge than simulating climate snapshots realistically, such as for the Last Glacial Maximum (LGM) (Yoshimori et al., 2002;Lunt et al., 2013;Colleoni et al., 2014a;Rachmayani et al., 2016).

Most efforts so far, with the notable exception of Ziemen et al. (2019), have used earth system models of intermediate complexity, EMICs, (Ganopolski and Brovkin, 2017;Ganopolski et al., 2010;Stap et al., 2014;Vizcaino et al., 2015;Calov et al., 2005;Heinemann et al., 2014;Willeit et al., 2019) or ice-sheet models (ISMs) coupled to statistical relationships, based on a set of coupled general circulation model (CGCM) timeslice runs (Abe-Ouchi et al., 2013;Colleoni et al., 2014b) to simulate the transient evolution of the coupled atmosphere-ocean-ice-sheet system. Bi-directional coupling between climate components and the ice-sheets, typically not captured in offline ice-sheet simulations (Born et al., 2010;Dolan et al., 2015;Koenig et al., 2015), is crucial in representing important feedbacks such as the ice albedo (Abe-Ouchi et al., 2013), elevation-desertification (Yamagishi et al., 2005) and the stationary wave – ice-sheet (Roe and Lindzen, 2001) feedbacks. Furthermore, it has been argued that the interaction between ice-sheets and ocean circulation (Timmermann et al., 2010;Rahmstorf, 2002;Knutti et al., 2004), and the resulting effects on the marine carbon cycle (Gildor and Tziperman, 2000;Menviel et al., 2012;Stein et al., 2020) can play a first-order role in shaping the climate evolution of the Quaternary on millennial and orbital timescales.

Glacial inceptions from warm mean states (interglacials) to cold mean states (glacials) over relatively short periods represent a bifurcation of the climate system and climate models have been shown to struggle in realistically simulating them (Calov and Ganopolski, 2005;Colleoni et al., 2014b). The glacial inception that has been studied most extensively is the one starting from the end of Last Interglacial (LIG, 125ka), corresponding to MIS 5a (Calov et al., 2005;Capron et al., 2017;Clark and Huybers, 2009;Crucifix and Loutre, 2002;Kubatzki et al., 2000;Nikolova et al., 2013;Otto-Bleisner et al., 2017;Pedersen et al., 2017). To our knowledge the penultimate interglacial, MIS 7 (240ka-170ka), has not received as much attention in ice-sheet modeling. MIS 7 (Fig.1c and 1d) is the coldest interglacial occurring after the Mid Brunhes Event (MBE, ~430k) (Colleoni and Masina, 2014) with an intensity comparable to typical pre-MBE interglacials (Pages, 2016). Furthermore, CO_2 concentrations were lower than 260 ppmv for most of MIS 7. Contrary to the classic sawtooth pattern of the Earth's glacial cycle (gradual buildup and fast termination of ice sheets within 80,000-120,000 years) (Clark et al., 2009;Hays et al., 1976), the global ice volume during MIS 7e-7c increased rapidly and then decreased rapidly by around 60 m of global sea level equivalent (SLE, relative to present day) within a period of 20 ky (thousand years) (Cheng et al. (2016), Fig. 1). This is the fastest such glaciation and deglaciation transition during the last 800 ky (Waelbroeck et al., 2002;Lisiecki and Raymo,

https://doi.org/10.5194/cp-2020-46
Preprint. Discussion started: 27 March 2020

2005;Bintanja et al., 2005) although the last deglaciation had a sea level rise of ~100m in 10ky, which makes it an interesting test-case for coupled climate-ice-sheet models. Subsequently, the system stayed in a relatively stable interglacial state and descended into the next glacial state at the end of MIS 7a (~190ka) into MIS 6e. In this paper, we follow the lettering convention of MIS substages as suggested by Railsback et al. (2015). In summary, the climate system started from an interglacial and went into a glacial state for both MIS 7e-7d (235-225ka) and MIS 7a-6e (190-180ka) transitions, but bounced back to the interglacial state only for the MIS 7d-7c (225-215ka) state and not for MIS 6e-6d (180-170ka). The drivers of this unique phasing and amplitude of sea level high stands during MIS 7 still remain elusive. Both periods of pre-inception (MIS 7e-7d and 7a-6e) have similar orbital forcings and so do the periods post-inception (MIS 7d-7c and 6e-6d). But the CO_2 values differ by ~40ppmv. Although the CO_2 trends are similar over pre-inception, they differ in the post-inception times (Fig. 4a, Lüthi et al. (2008)). The CO_2 values rise steeply over MIS 7d-7c but stay low during MIS 6e-6d.

Most simulations struggle in realistically simulating the whole of MIS 7. Previous studies focusing on the MIS 7 have modeled MIS 7e and MIS 7a-7c as separate interglacials. For instance, Yin and Berger (2012) and Colleoni et al. (2014a) have simulated the climate during MIS 7e using LOVECLIM (Goosse et al., 2010) and CESM (Gent et al., 2011) respectively, and compared it to that during MIS 5. While Yin and Berger (2012) report the insolation-induced cooling during MIS 7e to be the primary reason for it being a cold interglacial, Colleoni et al. (2014a) suggest that 70% of the cooling over the Northern Hemisphere (NH) in MIS 7e compared to MIS 5 can be explained by CO_2 forcings. Further, Colleoni et al. (2014b) used CESM outputs to force an offline 3-D ice-sheet model (ISM), Grenoble Ice Shelf and Land Ice model (Ritz et al., 2001), and they were not able to produce as realistic results for MIS 7 as they could for MIS 5. Ganopolski and Brovkin (2017) simulated the last 400ky using the CLIMBER-2 EMIC (Petoukhov et al., 2000) coupled with the SICOPOLIS ISM (Greve, 1997). When forced with both orbital and CO_2 variations, they reported an exaggerated inception at MIS 6e (~180ka) followed by an overshoot to interglacial levels at MIS 6d (~160ka), while forcing with just orbital variations led to a much weaker glacial inception at MIS 6e. More recently, Willeit et al. (2019) performed transient simulations using the previous setup (CLIMBER-SICOPOLIS) forced with orbital, regolith removal and volcanic outgassing and also showed an overshoot to interglacial levels after the glacial inception of MIS 6e.

Our study presents transient simulations over the MIS 7-6 period which use a novel bidirectionally coupled 3-dimensional EMIC-ISM framework (LOVECLIM-PSUIM) with interactive ice sheets in both hemispheres. Using multiple ensembles, we test the sensitivity of the simulation to different forcing and model parameters. By comparing the MIS 7e-7c and MIS 7a-6d transitions, we investigate the relative role of orbital and CO_2 forcings on glacial inceptions and terminations. We also look at different climate-ice sheet feedbacks and local processes that induce a bifurcation in the system and can show abrupt changes in the climate-cryosphere system such as those in the Atlantic Meridional Overturning Circulation (AMOC).

In Sect. 2, the individual components of our coupled model and the coupling framework are described, along with a list of the experiments. Next, the main results are presented in Sect. 3, including multi-ensemble simulations of ice sheet evolution, effects of orbital and CO_2 forcings pre and post glacial inception, abrupt changes in the climate-cryosphere system and the existence of multiple ice sheet equilibrium states. We conclude with a discussion of the key results and their implications for other glacial cycles along with key deficiencies in the current setup and possible solutions for future simulations.

https://doi.org/10.5194/cp-2020-46
Preprint. Discussion started: 27 March 2020

Climate of the Past Discussions
Open Access
EGU

2 Methods

We perform a series of transient glacial inception simulations covering the period from 240-170 ka using the bi-directionally coupled LOVECLIM-PSUIM system, henceforth called *LOVECLIP*. Both LOVECLIM (Friedrich et al., 2016;Nikolova et al., 2013;Timmermann and Friedrich, 2016;Timmermann et al., 2014;Yin and Berger, 2012) and the Penn State University Ice sheet Model, PSUIM (DeConto and Pollard, 2016;Gasson et al., 2018;Pollard et al., 2015;Tigchelaar et al., 2018), have been extensively used for simulating past and future climate. The individual components of the modelling framework as well as their coupling strategy are described below.

2.1 LOVECLIM

LOVECLIM is a three-dimensional Earth System Model of Intermediate Complexity with atmosphere, ocean, sea ice and vegetation models coupled together (Goosse et al., 2010). The atmospheric component of LOVECLIM, ECBilt (Opsteegh et al., 1998), is a spectral T21 ($5.625° \times 5.625°$) quasi-geostrophic model with three vertical levels including a parameterization of ageostrophic terms. The effect of CO_2 variations with respect to the reference CO_2 concentration (365ppm) on the longwave radiation flux is scaled up by a factor α, to account for the low default sensitivity of ECBilt to changes in CO_2 concentrations (Friedrich and Timmermann, 2020;Timmermann and Friedrich, 2016). α is determined based on transient past and future simulations. The ocean component, CLIO (Goosse and Fichefet, 1999), is a free-surface primitive-equation ocean general circulation model with $3° \times 3°$ horizontal resolution and 20 vertical levels; which is further coupled to a thermodynamic-dynamic sea ice model. Additionally, an iceberg model is employed that integrates iceberg trajectories (based on Coriolis force, air-water-sea ice drag, horizontal pressure gradient and wave radiation) and melt (depending on basal plus lateral melt and wave erosion along individual iceberg pathways) (Schloesser et al., 2019;Bigg et al., 1997). The atmosphere-ocean coupling is based on the freshwater, heat and momentum flux exchanges. The Bering Strait is opened and closed interactively depending on global mean sea level height. Specifically, its parameterized transport (is multiplied with a constant that is zero for sea levels lower than – 50 m meters and linearly increases to 1 as global sea level rises to -25 m relative to present day. The terrestrial biosphere component of LOVECLIM, VECODE (Brovkin et al., 1997), estimates the evolution of vegetation cover (fraction of grass, trees and desert) over each land grid cell not covered by ice.

2.2 PSUIM

PSUIM is a hybrid ice-sheet-ice-shelf model that combines the scaled shallow ice and shallow shelf approximations (Pollard and DeConto, 2012b). It has been shown to reasonably capture both slow and fast flowing grounded ice regimes as well as floating ice shelves while being simpler and more computationally efficient than Full-Stokes or Higher-Order models. The model also accounts for free grounding-line migration based on a sub-grid parameterization that calculates ice fluxes at the grounding line based on Schoof (2007). PSUIM calculates the surface energy and mass balances, by including the temperature and radiation contributions, to solve for surface melting and freezing (Robinson et al., 2010;Van Den Berg et al., 2008). Specifically, the energy flux available for melting ($dE > 0$) or refreezing ($dE < 0$) is given by:

$$dE = b(T - T_o) + (1 - a)Q - m, \quad (1)$$

where constant $b = 10\, Wm^{-2}K^{-1}$, T is the surface air temperature, T_o the freezing point, a the albedo, Q the surface incoming short wave radiation, and parameter m a constant (see Sect.2.3). The albedo is linearly interpolated between values for no snow ($a_{ns} = 0.5$), wet snow ($a_{ws} = 0.6$), and dry snow ($a_{ds} = 0.8$),

$$a = (1 - r_s)a_{ns} + r_s[r_l a_{ws} + (1 - r_l)a_{ds}], \quad (2)$$

where r_s is the snow covered area fraction and r_l the ratio between liquid water contained in the snow mass and the maximum embedded liquid capacity. The parameter 'm' appears in Eq. (1) represents net upwards infrared radiation from a solid surface

https://doi.org/10.5194/cp-2020-46
Preprint. Discussion started: 27 March 2020

Climate of the Past Discussions

at temperature T_o to the atmosphere, plus a constant correction for other simplifications in Eq. (1) and has units of Wm^{-2}.The surface mass balance is then calculated based on snow fall (which is calculated locally based on total precipitation and temperature) and melting/refreezing based on dE.

Calving is primarily parameterized depending on the ice shelf flow divergence. The model also includes parameterizations for surface meltwater and rainfall-driven hydrofracturing and the structural failure of tall sub-aerial ice cliffs, which produce strong ice retreat in Antarctic marine basins needed to explain past high sea level stands suggested by geologic data (DeConto and Pollard, 2016;Pollard et al., 2015). The sea level dependence is implemented by the formulation of boundary processes, such as calving, flotation of ice, grounding line dynamics and sub-grid pinning by bedrock bumps, which also affects the grounding line flux (Schoof, 2007). PSUIM is used to simulate ice sheets in both the hemispheres. The bedrock deformation is calculated by an ELRA (Elastic Lithosphere Relaxing Asthenosphere) model, assuming a bedrock density of 3370 kgm^{-3} and an isostatic asthenospheric relaxation time of 3000 years (Pollard and DeConto, 2012b). The basal sliding velocity is defined as in Pollard and DeConto (2012b) and depends on the basal sliding coefficient:

$$\widetilde{u_b} = C'|\tau_b|^{\mu-1}\widetilde{\tau_b} \,, \tag{3}$$

where $\widetilde{u_b}$ is the basal sliding velocity, $\widetilde{\tau_b}$ is the basal stress; μ is the basal sliding exponent (=2); C' is the basal sliding coefficient which is a function of the basal homologous temperature:

$$C' = (1-r)C_{froz} + rC(x,y) \,, \tag{4}$$

with $r = max\big[0, min[1, (T_b + 3)/3]\big]$; where T_b(℃) is the basal homologous temperature relative to the pressure melting point ($T_m = -0.000866h$, h being the ice thickness in m); and $C_{froz} = 10^{-20}\mathrm{m\ yr^{-1}Pa^{-2}}$ (which cannot be zero to avoid numerical inconsistencies but is small enough to allow essentially no sliding). For Antarctica, the sliding coefficient $C(x,y)$ is deduced from the inverse modelling approach of Pollard and DeConto (2012a). For the NH, a binary sliding coefficient map is used with higher sliding over present-day oceans ($C(x,y) = 10^{-6}\mathrm{m\ yr^{-1}Pa^{-2}}$ representing deformable sediments), and low sliding over present-day land ($C(x,y) = 10^{-10}\mathrm{m\ yr^{-1}Pa^{-2}}$ representing non-deformable rock).The model was tested at two resolutions for each hemisphere; for the NH, a longitude-latitude grid is used at either $1 \times 0.5°$ or $0.5 \times 0.25°$, and for Antarctica, a polar stereographic grid is used at either 40×40 km or 20×20 km. No significant differences in the results using the two resolutions were noticed for either hemisphere. All the results presented in this paper use $1 \times 0.5°$ for the NH and 40×40 km for Antarctica.

2.3 LOVECLIP

Figure 2 shows the coupling algorithm employed in the current setup to exchange information across LOVECLIM and PSUIM, between alternating climate model and ice sheet runs (chunks). LOVECLIM chunks of length T_L alternate with PSUIM chunks of length T_P ($\geq T_L$). Here we define the acceleration factor $N_A = T_P/T_L$. An earlier version of this coupling algorithm was used by Heinemann et al. (2014) for a different ISM (Ice sheet model for Integrated Earth system Studies (Saito and Abe-Ouchi, 2004) that was active only in the NH and did not include ice shelf-dynamics. The coupling strategy has the advantage of using asynchronous coupling to speed up climate simulations at millennial to orbital timescales (Friedrich et al., 2016;Tigchelaar et al., 2018;Timm and Timmermann, 2007;Timmermann and Friedrich, 2016). The fidelity of using the acceleration factor depends on how quickly the variables of interest equilibrate to the slowly evolving external boundary conditions. Preliminary experiments (not shown) with different acceleration factors suggest that model results do not change significantly when $N_A \leq 5$.

https://doi.org/10.5194/cp-2020-46
Preprint. Discussion started: 27 March 2020


Climate of the Past Discussions

PSUIM uses surface air temperature, precipitation, solar radiation, and ocean temperature at 400m depth as inputs from LOVECLIM. The surface temperature and precipitation outputs from LOVECLIM which are used for the PSUIM surface mass balance are bias-corrected in the coupler, following Pollard and DeConto (2012b) and Heinemann et al. (2014).

$$T(t) = T_{LC}(t) + T_{obs} - T_{LC,PD} \quad (5)$$

$$P(t) = P_{LC}(t) \times P_{obs}/P_{LC,PD} \quad (6)$$

where T is monthly surface air temperature and P is monthly precipitation forcing from LOVECLIM at timestep t. Subscripts 'LC', 'obs' and 'LC, PD' refer to LOVECLIM chunk output, observed present day climatology, and LOVECLIM present day control run, respectively. The observed present day climatology is obtained from the European Centre for Medium-Range Weather Forecasts reanalysis dataset, ERA-40 (Uppala et al., 2005). The annual mean of the monthly mean bias correction terms $T_{obs} - T_{LC,PD}$ and $P_{obs}/P_{LC,PD}$ are presented in Figure S1. Furthermore, for surface temperature T, a lapse-rate correction of 8°C km^{-1} is applied to account for differences between LOVECLIM orography and PSUIM topography and precipitation is multiplied by a Clausius–Clapeyron factor of $2^{\frac{\Delta T}{10^{\circ}C}}$, with ΔT being the temperature lapse-rate correction, to account for the elevation desertification effect (DeConto and Pollard, 2016).

LOVECLIM orography and surface ice mask are updated based on the evolution of ice sheets and bedrock elevation from PSUIM. Each grid cell of ECBilt and VECODE is defined as either ice-free or ice-covered (not fractionally covered); it is ice-covered if more than half of the cell has more than 10 m of ice in the finer PSUIM cells that lie within the LOVECLIM cell, thus changing the ground albedo to ice albedo. Basal melting and liquid runoff from PSUIM is discharged via LOVECLIM's runoff masks in both hemispheres; while the calving flux is channeled into CLIO's iceberg model (Schloesser et al., 2019;Jongma et al., 2009) in the Southern Hemisphere (SH) and as an iceberg melt flux in the NH (Schloesser et al., 2019).

The contributions of the ice sheets to global sea level changes are calculated independently for the two hemispheres in PSUIM, and the net sea level change is used for the next chunk of ice model run. Note, however, that LOVECLIM does not see the change in sea level, and the ocean bathymetry and land-sea mask (with the exception of the Bering Strait opening and closing) are not updated in the coupling framework. Our coupled simulations use the LGM bathymetry and land-sea mask throughout the entire transient simulation.

2.4 Experiments

The LOVECLIP experiments are initialized using present day ice sheet conditions and spun up using orbital and greenhouse gas (GHG) forcings of 240 ka for a period of 10ky. The model equilibrates to an ice sheet distribution in the NH corresponding to -20m SLE, implying an open Bering Strait. From these initial conditions, LOVECLIP is run forward with two transient forcings: Orbitally induced solar insolation variations following Berger (1978); and time-varying atmospheric GHG concentrations measured from the European Project for Ice Coring in Antarctica Dome C ice core (Loulergue et al., 2008;Lüthi et al., 2008;Schilt et al., 2010). Two additional sets of experiments are run to discern the independent effects of the two primary forcings: (1) Time varying orbital forcing with constant GHG concentration (set at its value for 240 ka), and (2) Constant orbital forcing (set at the orbit for 240 ka) and time varying GHG concentrations.

All the experiments presented in the paper are conducted with an acceleration factor $N_A = 5$. Ensembles of the full forcing experiments with different GHG sensitivities (α, Sect. 2.1) and melt parameterizations (m, Sect. 2.2) are also run to test the sensitivity of the model to different sets of parameters. Higher α leads to a larger response of ice to changes in CO_2

https://doi.org/10.5194/cp-2020-46
Preprint. Discussion started: 27 March 2020

concentrations. And generally speaking, higher values of m lead to stronger buildup and weaker melting of ice during interglacial climates. All of the experiments are listed in Table 1.

3 Results

3.1 Overview of multi-parameter ensemble coupled simulations

Figure 3 shows the simulated ice volume in SLE (m). Figure 3a shows the most realistic simulation (referred to as baseline simulation BLS, experiment 1 in Table 1) in comparison to the sea level reconstructions of Spratt and Lisiecki (2016). Parameter sensitivities will be further discussed below. The model captures the overall trajectory of ice volume evolution reasonably well. Although the extreme glaciation-deglaciation event of MIS 7e-7d-7c is very well simulated, the glaciation into MIS 6 is delayed by ~3ky (191ka instead of 194ka). This lag can be also found in other studies such as and Ganopolski and Calov (2011) and Ganopolski and Brovkin (2017), and we could not identify a reason for this discrepancy between simulations and reconstructions. Only a selection of ensembles is shown here that depict the sensitivity of the model to physical and model parameters in a representative way. Higher climate sensitivity (α) leads to a much faster and stronger glacial inception and termination at the MIS 7e-7d-7c transition, in response to the time-varying orbital forcing and CO_2 changes (Fig. 3b). Increasing the value of m (Eq. (1)) leads to a deeper inception and much weaker termination (Fig. 3c). The most realistic simulation is obtained for $\alpha = 2$ and $m = 125$ Wm^{-2}. Unless otherwise mentioned, all results presented in this study are from this particular ensemble member (labelled BLS). Clearly, if either the climate sensitivity (α) or the parameter in the linear energy balance model (m) exceed certain thresholds, our model simulates an unrealistic runaway glaciation. The underlying model physics involved in this feature will be described further below.

3.2 Ice sheet evolution

The rapid waxing and waning of ice sheets during the MIS 7e-7d-7c transition is presented in terms of maps of ice height and basal velocities in Fig. 4. Our simulations suggest that the primary contribution to the ice volume evolution during MIS 7-6 came from the NH (blue line in Fig. 4b). SH only contributes around 10m SLE during the interstadial of MIS 7c (red line in Fig. 4b). In the short transition (~10ky) from MIS 7e (235ka, Fig. 4c) to MIS 7d (226ka, Fig. 4e), ~4km thick Laurentide and ~3km thick Cordilleran ice sheets are built up over the NH. Our simulation shows the Eurasian ice sheet builds up much less during this period. Although the contribution of Antarctica during MIS 7d is less than 5m, the Filchner-Ronne ice shelf spreads further out into the Weddell Sea (Fig. 4f, ice shelves do not directly contribute to sea level change). This quick glaciation event coincides with decreasing NH summer insolation and CO_2 forcings. Although NH insolation reaches a minimum at ~230ka and starts rising again, CO_2 stays higher than 220ppm till ~227ka and drops only just before MIS 7d (~226ka, Fig. 4a). Next, there is a rapid deglaciation event corresponding to the steep increase in both orbital and GHG forcings over MIS 7d to 7c. Our model successfully simulates ice sheet retreat by the saddle collapse of Laurentide and Cordilleran splitting (Gregoire et al., 2012). While some studies have suggested the sea level peak at MIS 7c to be lower (Dutton et al., 2009) than those at MIS 7e and 7a, our model simulates MIS 7c to be the highest peak in MIS 7 with marked deglaciation of the Laurentide and Cordilleran, reduced Innuitian, Greenland, and small Icelandic and Norwegian ice sheets (Fig. 4g), along with a reduced West Antarctic ice sheet (Fig. 4h). The highest contribution of SH to MIS 7 of ~10m (Fig. 4b and 4h) occurs during MIS 7c. After a relatively stable interglacial state till MIS 7a, the system moves into the next glacial and reaches a glacial equilibrium state. At the end of the simulation, our model simulates a bigger Laurentide and relatively smaller and detached Cordilleran as the model glaciates into MIS 6 (Fig. 4i). Although studies of NH reconstructions such as Svendsen et al. (2004) and more recently,

https://doi.org/10.5194/cp-2020-46
Preprint. Discussion started: 27 March 2020

265 Batchelor et al. (2019), have suggested a larger Eurasian ice sheet over the MIS 6 period (160-140ka), our simulations show a persistent Fenno-Scandian ice sheet and a relatively small Eurasian ice sheet at 170ka.

3.3 Effects of orbital and GHG forcings

Figure 5 shows the effects of the individual orbital and GHG forcings on the simulated ice volume. As expected, keeping both
270 orbital and GHG forcings fixed at 240ka values leads to no change in the ice volume (control run, dashed line). Forcing with only GHG variations alone (red line) leads to a small cooling trend compared to the control run but does not simulate any glacial inceptions. On the other hand, forcing with orbital variations only (blue line) does simulate glacial inceptions, albeit only half of the magnitude over MIS 7e-7d-7c, and the system does not glaciate completely at MIS 6 (170ka). This can be attributed to the fact that the NH summer insolation at 170ka is relatively strong at almost interglacial levels (Fig. 1a and 4a)
275 and that the MIS 6 inception might have been controlled by the low GHG values. Our orbital-only simulation is also very similar to the run of Ganopolski and Brovkin (2017) which was forced with orbital variations only with a constant CO_2 concentration of 240ppm (ONE_240 experiment, green line in their Fig. 8). Although they simulated the 7e-7d-7c transition well, their orbital-only run did not glaciate successfully into MIS 6. This suggests that glacial inceptions, at least over the MIS 7-6 period, are primarily controlled by orbital forcings, discussed further in the next Sect. 3.4, supporting previous studies of
280 Ganopolski and Brovkin (2017), Yin and Berger (2012) and Ganopolski and Calov (2011). However, it is imperative to restate that orbital forcings alone cannot force the system into the MIS 6 glacial, and low GHG values over 180-170ka are crucial for the MIS 6 inception. Please note that all four runs in Fig. 5 were conducted with $\alpha = 2$ and $m = 125$ Wm^{-2}, and different values of the parameters might have led to different ice sheet evolutions and different sensitivities with respect to orbital and greenhouse gas forcing.

285

3.4 Effects of forcings pre and post inception

In Figures 4a and 4b we highlight two 20ky periods in shading (235-215ka and 190-170ka) in dark and light grey colors. The dark grey periods (235-225ka and 190-180ka) are characterized by minimum values of NH summer insolation and the buildup of ice volume. The light grey marked periods (225-215ka and 180-170ka) correspond to peak summer insolation. In case of
290 MIS 7d-7c, we observe a glacial termination, whereas the MIS 6e-6d period is characterized only by small changes in ice volume. By compositing the climate evolution over the NH for these two periods, we can further explore the reasons for the varying ice sheet responses during the MIS 7d-7c and the MIS 6e-6d periods (Figure 6). MIS 7e-7d-7c (MIS 7a-6e-6d) data are marked by dashed (solid) lines. Figure 6a shows the similarity of the orbital forcings during both periods. In contrast, their respective CO_2 evolutions are very different (Figure 6b). Even though the CO_2 values are markedly different in the first part
295 (10ky) of the two periods (Fig. 6b), the simulated total NH ice volume evolution is quite similar (Fig. 6c). This highlights the relevance of orbital forcing during glacial inceptions. However, in the second half of the composite figure and in spite of similar orbital forcing, we see a very different behavior, with one successful glacial termination, due to increasing CO_2 concentrations (dashed line), and an aborted termination during MIS 6e-6d (180-170ka, solid line), due to flat-lined glacial CO_2 values (Fig. 6a-6c). Likewise, the global average surface temperature evolution is similar for the pre-inception case but
300 different for the post-inception cases (Fig. 6d). Any difference in the patterns within the two time periods of pre-inception and those of post-inception periods can be attributed to the difference in CO_2 evolution.

However, unlike ice volume and surface temperature evolutions, the time evolution of the Atlantic Meridional Overturning Circulation (AMOC) is very similar for both periods (Fig. 6e). Even over the 180-170 ka period in the post-inception case of
305 high NH ice volume, the AMOC recovers almost to its full interglacial state. Figure 6 also shows the evolution of the different

https://doi.org/10.5194/cp-2020-46
Preprint. Discussion started: 27 March 2020

mass balance terms for both the pre-inception and post-inception cases. Accumulation and ablation depend on the surface temperature over and the extent of the ice sheets (Fig. 6f and 6g). As ice sheets grow further equatorward, they come in contact with warmer moist air leading to a positive feedback on the ice growth because of higher moisture carrying ability of warm air. But higher temperatures also lead to higher ablation because of increased surface melting. Furthermore, as the ice sheet grows in height, accumulation decreases because of the elevation desertification effect (DeConto and Pollard, 2016), while ablation reduces due to the lapse rate. Although accumulation and ablation can change both in and out of phase, the delicate interplay of leads and lags between them governs the sign of the net surface mass balance (Fig. 6h). For the pre-inception cases, accumulation leads ablation producing a net positive surface mass balance (SMB) till it reaches peak glaciation for both time periods. Subsequently, the SMB turns negative only for the second half of the 7e-7d-7c period and not the 7a-6e-6d period (Fig. 6e-g). The deglaciation is initiated by increased ablation around 4ky after the inception at MIS 7d (~221ka, dashed line in Fig. 6g), corresponding to the increasing CO_2 (dashed line in Fig. 6b), followed by a decrease in accumulation (dashed line in Fig. 6f) that can be attributed to the ice sheets retreating further north. Also, the ablation over 7d-7c (225-215ka, Fig. 6g) contains an additional saddle collapse (Gregoire et al., 2012) contribution when the Laurentide and Cordilleran ice sheets separate (Fig. 4e) leading to higher surface melting followed by rapid melting of both ice sheets. This shows up as the sharp spike in ablation around 15ky of the 7e-7d-7c transition (~220ka, Fig. 6g) and amounts to the steep negative SMB in Fig. 6h. Together with the negative subshelf melting spike in Fig. 6i, this leads to a ~10m rapid increase in SLE around 219.5ka in Fig. 6c and Fig. 4b. Such abrupt changes are discussed further in Sect. 3.5. Although the Laurentide and Cordilleran ice sheets separate during the period 180-170ka, the net SMB does not exhibit a negative trend. This can be attributed to the low CO_2 value (<200ppmv) leading to temperatures low enough (Fig. 6d) to avoid ablation even if the Laurentide extends equatorward (Fig. 6g). Furthermore, the southern extent of the Laurentide can lead to changes in circulation patterns that can alter the SMB (discussed in Sect. 3.6).

3.5 Abrupt changes in the coupled climate-cryosphere system

The advantage of using a fully coupled framework is that feedbacks in the climate-ice-sheet system can be simulated and understood. Here we focus on the feedbacks that lead to exceptionally fast ice loss around 220ka during the MIS 7d-7e transition; with anomalies of different climate variables during this transition for 220.5ka, 220ka and 219.5ka shown in Fig. S2, S3 and S4 respectively. A 3˚C anomalous subsurface warming over Baffin Bay at 220.5k (Fig. S2b) causes the Laurentide ice-sheet to melt from the east (Fig. S2a, S2d and S2f). At the same time, as the very western margin of the Laurentide starts thinning, it becomes a floating ice shelf instead of being grounded, as can be seen by the grounding line and ice velocities in Fig. S2a. This is because as the ice-sheet retreats, land areas below sea-level become exposed, which are connected to ocean points. PSUIM then assumes that the points will become ocean points and therefore the thinning western Laurentide changes from a grounded ice sheet to an ice shelf (grounding line in Fig. S2a). This shelf on the western margin has a surface temperature relatively warmer than the rest of Laurentide (Fig. S2c) and shows a weakly positive to negative SMB anomaly (Fig. S2d and S2f). The surface melting in the ice free region between Laurentide and Cordilleran ice sheets leads to an expanded surface ablation zone (Fig. S2d) and accelerated mass balance-elevation feedbacks (Weertman, 1961). This sort of accelerated melting due to the saddle effect has previously been documented by Gregoire et al. (2012) for the Meltwater Pulse events. These anomalies over the western Laurentide amplify over the next 500 years. Alongside warmer temperatures over the eastern Laurentide, the western Laurentide also shows anomalies up to +2˚C during 220ka (Fig. S3c). Not only the floating shelves, but also grounded regions of the western Laurentide show negative SMB anomaly (Fig. S3d) and basal sliding (Fig. S3a). Further, relatively warm subsurface ocean waters (>-1˚C) seeps along the west bank of Hudson Bay leading to a more pronounced negative mass balance (Fig. S3d). This shows up as a spike in the subsurface ocean melt values in Fig. 6i. Although the model simulates sub shelf melting along western Hudson Bay, we did not find any geologic evidence of such subsurface

https://doi.org/10.5194/cp-2020-46
Preprint. Discussion started: 27 March 2020

Climate of the Past Discussions
Open Access
EGU

melting around 219.5ka. It is also worth mentioning that our setup does not simulate forebulges or other specific mechanisms modelled by more comprehensive full-Earth models. But Tigchelaar et al. (2018) have reported such changes in mass balance arising due to changing of ice sheets to ice shelves near the grounding line. These surface and sub-surface melting processes of the Laurentide trigger a rapid retreat of the ice-sheet within the next 0.5ky (Fig. S4), accounting for the ~10m SLE rise in 0.5ky (Fig. 6c and 4b).

3.6 Climate-ice sheet bifurcations and multiple equilibria

In Figure 3 we found a strong sensitivity of the simulated ice-sheet evolution to the energy balance parameter (m). Experiments with values of $120\ Wm^2 \leq m \leq 130\ Wm^2$ lead to a realistic glacial inception and termination over MIS 7e-7d-7c. Values lower than this do not simulate the full magnitude of glaciation, while values higher than this threshold cause a rapid glacial build-up and a run-away effect with unrealistic growth of ice-sheets. Even though we did not run steady-state experiments, this behavior is reminiscent of a saddle node bifurcation. Bifurcations in the climate-cryosphere system in response to astronomical forcings have been previously documented by studies such as Paillard (1998), Calov et al. (2005), Ashwin and Ditlevsen (2015) and Ganopolski et al. (2016). While previous studies have used empirical models or coupled ice sheet models to understand such bifurcations based solely on forcing and ice volume thresholds, here we investigate the changes in climate teleconnections and stationary wave patterns that can arise from slightly different ice sheet distributions, to explain the inherent mechanisms of the simulated bifurcation. Figure 7a shows two simulations that have a very similar evolution and capture the 7e-7d-7c transition realistically but show very different trajectories after the inception at MIS 6. Both ensembles were run with the same α=2 but different m=125 Wm^{-2} and m=130 Wm^{-2}. While one leads to a stable inception into MIS 6 (blue, m=125 Wm^{-2}), the other leads to a runaway glaciation (black, m=130 Wm^{-2}) with a total ice volume of 180 m SLE at 160ka (Fig. 7a). We assume that the bifurcation of the trajectories happens around 180ka, where the difference in ice volume between the two ensembles is only 10m SLE. Although the Cordilleran looks very similar, the Laurentide is slightly bigger and has a higher and wider dome at the southern tip in the runaway simulation (Fig. 7c compared to 7b). Also, the Laurentide and Cordilleran are connected further south and this bridge is also higher in the runaway simulation (Fig. 7e). This higher bridge and Laurentide ice sheet locally lead to a surface cooling and thus to a net positive surface mass balance (Fig. 7f and 7g). Also, an anomalous cyclonic circulation develops south of the Laurentide in the runaway case leading to a positive net budget just south of the Laurentide (Fig. 7g), while the positive budget is much further away from the Laurentide in the stable run (Fig. 7f). Westerly storm tracks veered further south by a weaker Aleutian Low and a stronger North Pacific High, as reported by Oster et al. (2015) for the LGM, bring in moisture towards the southern end of the Laurentide. The shape of the Laurentide and the saddle in the stable run cause this jet stream to meander around and precipitate on the southeastern tip of the Laurentide (Francis and Vavrus, 2012) (Fig. 7h). These winds might also cause the moisture laden air from the Gulf of Mexico to precipitate just north of the Gulf of Mexico (Fig. 7h). But in the runaway run, the jet stream is more northerly and precipitates over the southwestern tip of Laurentide (Fig. 7i). The Laurentide ice-sheet extending further south causes the moist air from the Gulf of Mexico to also precipitate over the southwestern end of the Laurentide alongside the moist air from the jet stream intensifying further southwestward growth of the Laurentide. This southwestward growth of Laurentide in turn enhances the poleward moisture transport. These stationary wave feedbacks are similar to the ones described by Roe and Lindzen (2001). The atmospheric patterns strengthen over the next 10ky and the runaway run simulates ~30m SLE greater ice volume than the stable run (Fig. S5). The difference between the two runs at 180ka and 170ka are presented in Fig. S6.

https://doi.org/10.5194/cp-2020-46
Preprint. Discussion started: 27 March 2020

Climate of the Past Discussions
Open Access
EGU

4 Summary and Discussion

Modeling glacial cycles remains a key challenge, especially because of the two-way interactions between ice sheets and climate and the emerging possibility for multiple equilibrium states. The ice-volume evolution originates from a time-integration of small net mass balance terms (e.g. Fig. 6h), which themselves originate from the difference of large accumulation and ablation terms. Long-term orbital-scale integrations of such delicate net surface mass balances can further lead to an accrual of errors. Here we focused on the penultimate interglacial, MIS 7-MIS 6 which is characterized by intervals with both in-phase and out-of-phase orbital and GHG variations. This interesting period involves one of the fastest glacial build-ups and terminations, with SLE variations of up to ±60m within a period of 20ky. Due to the rapid response of the ice sheets to orbital and CO_2 forcings, this period serves as an excellent benchmark for coupled climate-ice sheet simulations. Our bidirectionally coupled three-dimensional climate-ice sheet model simulations with ice sheets and ice shelves represented in both hemispheres suggest that glacial inceptions are more sensitive to orbital variations, whereas terminations from deep glacial conditions need both orbital and CO_2 forcing to work in tandem over a narrow ablation zone at the southern margins of northern hemispheric ice sheets. We find that small changes in the Laurentide's ice distribution for similar total ice volumes can lead to a saddle node bifurcation of the system, which in turn determines whether the coupled trajectory will follow a deglaciation or a runaway glaciation pathway in response to the combination of forcings. This runaway glaciation can be explained in terms of a positive stationary-wave-ice sheet feedback in which ice topography-driven moisture transport from westerly storm tracks and the Gulf of Mexico leads to enhanced rainfall accumulation over the southern tip of the Laurentide, making it grow further southwestward.

Results also suggest that our coupled simulations are realistic over a narrow range of parameters, and are very sensitive to changes in parameter values that can produce starkly different trajectories. Potentially more realistic results could be obtained if the simulations were unaccelerated (which would be computationally very expensive), and from using more complex climate models that include stratification-dependent mixing in the ocean for instance. Also, the stationary wave feedback reported here could be a model dependent feature of LOVECLIM, given it has only three atmospheric levels, and so could vary with the choice of the climate model used. Furthermore, Glacial Isostatic Adjustment (GIA) processes captured only in comprehensive full-Earth models such as forebulges are not simulated in the ice-sheet model used here. Nevertheless, we would like to reiterate that simulating a trajectory is more difficult than conducting timeslice experiments, as climate and ice sheet components work on totally different timescales and a fine interplay of parameters can add up to very different equilibrium states.

Data Availability

The data that support the findings of this study are available from the corresponding author on request.

Author contributions

AT designed the research. DC, FS, MH and DP developed the model code. DC conducted the model simulations and analyzed the data. DC and AT prepared the manuscript with contributions from all the co-authors.

Competing interests

The authors declare no competing interests.

https://doi.org/10.5194/cp-2020-46
Preprint. Discussion started: 27 March 2020

Climate of the Past Discussions
Open Access
EGU

Acknowledgements

This research is supported by the Institute for Basic Science, South Korea (Grant No: IBS-R028-D1) and NSF Grant # 1903197. The simulations were conducted at the Center for High-Performance Computing at the University of Southern California.

https://doi.org/10.5194/cp-2020-46
Preprint. Discussion started: 27 March 2020

Climate of the Past Discussions
Open Access
EGU

References

Abe-Ouchi, A., Saito, F., Kawamura, K., Raymo, M. E., Okuno, J. i., Takahashi, K., and Blatter, H.: Insolation-driven 100,000-year glacial cycles and hysteresis of ice-sheet volume, nature, 500, 190-193, 2013.

Ashwin, P., and Ditlevsen, P.: The middle Pleistocene transition as a generic bifurcation on a slow manifold, Climate dynamics, 45, 2683-2695, 2015.

Batchelor, C. L., Margold, M., Krapp, M., Murton, D. K., Dalton, A. S., Gibbard, P. L., Stokes, C. R., Murton, J. B., and Manica, A.: The configuration of Northern Hemisphere ice sheets through the Quaternary, Nature communications, 10, 1-10, 2019.

Berger, A.: Long-term variations of daily insolation and Quaternary climatic changes, Journal of the Atmospheric Sciences, 35, 2362-2367, 1978.

Bigg, G. R., Wadley, M. R., Stevens, D. P., and Johnson, J. A.: Modelling the dynamics and thermodynamics of icebergs, Cold Regions Science and Technology, 26, 113-135, 1997.

Bintanja, R., van de Wal, R. S. W., and Oerlemans, J.: Modelled atmospheric temperatures and global sea levels over the past million years, Nature, 437, 125-125, 2005.

Born, A., Kageyama, M., and Nisancioglu, K. H.: Warm Nordic Seas delayed glacial inception in Scandinavia, Climate of the Past, 6, 817-826, 2010.

Brovkin, V., Ganopolski, A., and Svirezhev, Y.: A continuous climate-vegetation classification for use in climate-biosphere studies, Ecological Modelling, 101, 251-261, 1997.

Calov, R., and Ganopolski, A.: Multistability and hysteresis in the climate-cryosphere system under orbital forcing, Geophysical Research Letters, 32, 10.1029/2005gl024518, 2005.

Calov, R., Ganopolski, A., Claussen, M., Petoukhov, V., and Greve, R.: Transient simulation of the last glacial inception. Part I: glacial inception as a bifurcation in the climate system, Climate Dynamics, 24, 545-561, 10.1007/s00382-005-0007-6, 2005.

Capron, E., Govin, A., Feng, R., Otto-Bliesner, B. L., and Wolff, E. W.: Critical evaluation of climate syntheses to benchmark CMIP6/PMIP4 127 ka Last Interglacial simulations in the high-latitude regions, Quaternary Science Reviews, 168, 137-150, 2017.

Cheng, H., Edwards, R. L., Sinha, A., Spotl, C., Yi, L., Chen, S., Kelly, M., Kathayat, G., Wang, X., Li, X., Kong, X., Wang, Y., Ning, Y., and Zhang, H.: The Asian monsoon over the past 640,000 years and ice age terminations, Nature, 534, 640-646, 10.1038/nature18591, 2016.

Clark, P. U., Dyke, A. S., Shakun, J. D., Carlson, A. E., Clark, J., Wohlfarth, B., Mitrovica, J. X., Hostetler, S. W., and McCabe, A. M.: The last glacial maximum, science, 325, 710-714, 2009.

Clark, P. U., and Huybers, P.: Global change: Interglacial and future sea level, Nature, 462, 856-856, 2009.

Colleoni, F., and Masina, S.: Impact of greenhouse gases and insolation on the threshold of glacial inception, Annual Conference of the Societá Italiana per le Scienze del Clima, 2014,

Colleoni, F., Masina, S., Cherchi, A., and Iovino, D.: Impact of Orbital Parameters and Greenhouse Gas on the Climate of MIS 7 and MIS 5 Glacial Inceptions, Journal of Climate, 27, 8918-8933, 2014a.

Colleoni, F., Masina, S., Cherchi, A., Navarra, A., Ritz, C., Peyaud, V., and Otto-Bliesner, B.: Modeling Northern Hemisphere ice-sheet distribution during MIS 5 and MIS 7 glacial inceptions, Climate of the Past, 10, 269-291, 10.5194/cp-10-269-2014, 2014b.

Crucifix, M., and Loutre, F. M.: Transient simulations over the last interglacial period (126--115 kyr BP): feedback and forcing analysis, Climate Dynamics, 19, 417-433, 2002.

DeConto, R. M., and Pollard, D.: Contribution of Antarctica to past and future sea-level rise, Nature, 531, 591-591, 2016.

Dolan, A. M., Hunter, S. J., Hill, D. J., Haywood, A. M., Koenig, S. J., Otto-Bliesner, B. L., Abe-Ouchi, A., Bragg, F., Chan, W. L., Chandler, M. A., and others: Using results from the PlioMIP ensemble to investigate the Greenland Ice Sheet during the mid-Pliocene Warm Period, Climate of the Past Discussions, 11, 403-424, 2015.

Dutton, A., Bard, E., Antonioli, F., Esat, T. M., Lambeck, K., and McCulloch, M. T.: Phasing and amplitude of sea-level and climate change during the penultimate interglacial, Nature Geoscience, 2, 355-355, 2009.

Francis, J. A., and Vavrus, S. J.: Evidence linking Arctic amplification to extreme weather in mid-latitudes, Geophysical Research Letters, 39, 2012.

Friedrich, T., Timmermann, A., Tigchelaar, M., Timm, O. E., and Ganopolski, A.: Nonlinear climate sensitivity and its implications for future greenhouse warming, Science Advances, 2, e1501923-e1501923, 2016.

Friedrich, T., and Timmermann, A.: Using Late Pleistocene sea surface temperature reconstructions to constrain future greenhouse warming, Earth and Planetary Science Letters, 530, 115911, 2020.

Ganopolski, A., Calov, R., and Claussen, M.: Simulation of the last glacial cycle with a coupled climate ice-sheet model of intermediate complexity, Climate of the Past, 6, 229-244, 2010.

Ganopolski, A., and Calov, R.: The role of orbital forcing, carbon dioxide and regolith in 100 kyr glacial cycles, Climate of the Past, 7, 1415-1425, 2011.

Ganopolski, A., Winkelmann, R., and Schellnhuber, H. J.: Critical insolation–CO_2 relation for diagnosing past and future glacial inception, Nature, 529, 200, 2016.

Ganopolski, A., and Brovkin, V.: Simulation of climate, ice sheets and CO_2; evolution during the last four glacial cycles with an Earth system model of intermediate complexity, Climate of the Past Discussions, 1-38, 2017.

Gasson, E. G. W., DeConto, R. M., Pollard, D., and Clark, C. D.: Numerical simulations of a kilometre-thick Arctic ice shelf consistent with ice grounding observations, Nature communications, 9, 1510-1510, 2018.

Gent, P. R., Danabasoglu, G., Donner, L. J., Holland, M. M., Hunke, E. C., Jayne, S. R., Lawrence, D. M., Neale, R. B., Rasch, P. J., Vertenstein, M., and others: The community climate system model version 4, Journal of Climate, 24, 4973-4991, 2011.

Gildor, H., and Tziperman, E.: Sea ice as the glacial cycles' climate switch: Role of seasonal and orbital forcing, Paleoceanography and Paleoclimatology, 15, 605-615, 2000.

Goosse, H., and Fichefet, T.: Importance of ice-ocean interactions for the global ocean circulation: A model study, Journal of Geophysical Research: Oceans, 104, 23337-23355, 1999.

Goosse, H., Brovkin, V., Fichefet, T., Haarsma, R., Huybrechts, P., Jongma, J., Mouchet, A., Selten, F., Barriat, P. Y., Campin, J. M., Deleersnijder, E., Driesschaert, E., Goelzer, H., Janssens, I., Loutre, M. F., Morales Maqueda, M. A., Opsteegh, T., Mathieu, P. P., Munhoven, G., Pettersson, E. J., Renssen, H., Roche, D. M., Schaeffer, M., Tartinville, B., Timmermann, A., and Weber, S. L.: Description

https://doi.org/10.5194/cp-2020-46
Preprint. Discussion started: 27 March 2020

of the Earth system model of intermediate complexity LOVECLIM version 1.2, Geoscientific Model Development, 3, 603-633, 10.5194/gmd-3-603-2010, 2010.
Gregoire, L. J., Payne, A. J., and Valdes, P. J.: Deglacial rapid sea level rises caused by ice-sheet saddle collapses, Nature, 487, 219, 2012.
Greve, R.: A continuum--mechanical formulation for shallow polythermal ice sheets, Philosophical Transactions of the Royal Society of London A: Mathematical, Physical and Engineering Sciences, 355, 921-974, 1997.
Hays, J. D., Imbrie, J., and Shackleton, N. J.: Variations in the Earth's orbit: pacemaker of the ice ages, Science, 194, 1121-1132, 1976.
Heinemann, M., Timmermann, A., Elison Timm, O., Saito, F., and Abe-Ouchi, A.: Deglacial ice sheet meltdown: orbital pacemaking and CO 2 effects, Climate of the Past, 10, 2014.
Jongma, J. I., Driesschaert, E., Fichefet, T., Goosse, H., and Renssen, H.: The effect of dynamic–thermodynamic icebergs on the Southern Ocean climate in a three-dimensional model, Ocean Modelling, 26, 104-113, 2009.
Jouzel, J., Masson-Delmotte, V., Cattani, O., Dreyfus, G., Falourd, S., Hoffmann, G., Minster, B., Nouet, J., Barnola, J.-M., and Chappellaz, J.: Orbital and millennial Antarctic climate variability over the past 800,000 years, science, 317, 793-796, 2007.
Knutti, R., Flückiger, J., Stocker, T., and Timmermann, A.: Strong hemispheric coupling of glacial climate through freshwater discharge and ocean circulation, Nature, 430, 851-856, 2004.
Koenig, S. J., Dolan, A. M., De Boer, B., Stone, E. J., Hill, D. J., DeConto, R. M., Abe-Ouchi, A., Lunt, D. J., Pollard, D., Quiquet, A., and others: Ice sheet model dependency of the simulated Greenland Ice Sheet in the mid-Pliocene, Climate of the Past, 11, 369-381, 2015.
Kubatzki, C., Montoya, M., Rahmstorf, S., Ganopolski, A., and Claussen, M.: Comparison of the last interglacial climate simulated by a coupled global model of intermediate complexity and an AOGCM, Climate Dynamics, 16, 799-814, 2000.
Laskar, J., Robutel, P., Joutel, F., Gastineau, M., Correia, A., and Levrard, B.: A long-term numerical solution for the insolation quantities of the Earth, Astronomy & Astrophysics, 428, 261-285, 2004.
Lisiecki, L. E., and Raymo, M. E.: A Pliocene-Pleistocene stack of 57 globally distributed benthic δ18O records, Paleoceanography, 20, 2005.
Loulergue, L., Schilt, A., Spahni, R., Masson-Delmotte, V., Blunier, T., Lemieux, B., Barnola, J.-M., Raynaud, D., Stocker, T. F., and Chappellaz, J.: Orbital and millennial-scale features of atmospheric CH 4 over the past 800,000 years, Nature, 453, 383-383, 2008.
Lunt, D. J., Abe-Ouchi, A., Bakker, P., Berger, A., Braconnot, P., Charbit, S., Fischer, N., Herold, N., Jungclaus, J. H., Khon, V. C., and others: A multi-model assessment of last interglacial temperatures, Climate of the Past, 9, 699-717, 2013.
Lüthi, D., Le Floch, M., Bereiter, B., Blunier, T., Barnola, J.-M., Siegenthaler, U., Raynaud, D., Jouzel, J., Fischer, H., Kawamura, K., and others: High-resolution carbon dioxide concentration record 650,000--800,000 years before present, Nature, 453, 379-379, 2008.
Menviel, L., Joos, F., and Ritz, S.: Simulating atmospheric CO_2, 13C and the marine carbon cycle during the Last Glacial–Interglacial cycle: possible role for a deepening of the mean remineralization depth and an increase in the oceanic nutrient inventory, Quaternary Science Reviews, 56, 46-68, 2012.
Nikolova, I., Yin, Q., Berger, A., Singh, U. K., and Karami, M. P.: The last interglacial (Eemian) climate simulated by LOVECLIM and CCSM3, Climate of the Past, 9, 1789-1806, 2013.
Opsteegh, J. D., Haarsma, R. J., Selten, F. M., and Kattenberg, A.: ECBILT: A dynamic alternative to mixed boundary conditions in ocean models, Tellus A: Dynamic Meteorology and Oceanography, 50, 348-367, 1998.
Oster, J. L., Ibarra, D. E., Winnick, M. J., and Maher, K.: Steering of westerly storms over western North America at the Last Glacial Maximum, Nature Geoscience, 8, 201, 2015.
Otto-Bleisner, B. L., Braconnot, P., Harrison, S. P., Lunt, D. J., Abe-Ouchi, A., Albani, S., Bartlein, P. J., Capron, E., Carlson, A. E., Dutton, A., and others: The PMIP4 contribution to CMIP6--Part 2: Two interglacials, scientific objective and experimental design for Holocene and Last Interglacial simulations, Geoscientific Model Development, 10, 3979-4003, 2017.
Pages, P. I. W. G. o.: Interglacials of the last 800,000 years, Reviews of Geophysics, 54, 162-219, 2016.
Paillard, D.: The timing of Pleistocene glaciations from a simple multiple-state climate model, Nature, 391, 378, 1998.
Pedersen, R. A., Langen, P. L., and Vinther, B. M.: The last interglacial climate: comparing direct and indirect impacts of insolation changes, Climate Dynamics, 48, 3391-3407, 2017.
Petoukhov, V., Ganopolski, A., Brovkin, V., Claussen, M., Eliseev, A., Kubatzki, C., and Rahmstorf, S.: CLIMBER-2: a climate system model of intermediate complexity. Part I: model description and performance for present climate, Climate dynamics, 16, 1-17, 2000.
Pollard, D., and DeConto, R. M.: A simple inverse method for the distribution of basal sliding coefficients under ice sheets, applied to Antarctica, The Cryosphere, 6, 953-971, 10.5194/tc-6-953-2012, 2012a.
Pollard, D., and DeConto, R. M.: Description of a hybrid ice sheet-shelf model, and application to Antarctica, Geoscientific Model Development, 5, 1273-1295, 10.5194/gmd-5-1273-2012, 2012b.
Pollard, D., DeConto, R. M., and Alley, R. B.: Potential Antarctic Ice Sheet retreat driven by hydrofracturing and ice cliff failure, Earth and Planetary Science Letters, 412, 112-121, 2015.
Rachmayani, R., Prange, M., and Schulz, M.: Intra-interglacial climate variability: model simulations of Marine Isotope Stages 1, 5, 11, 13, and 15, Climate of the Past, 12, 677-695, 10.5194/cp-12-677-2016, 2016.
Rahmstorf, S.: Ocean circulation and climate during the past 120,000 years, Nature, 419, 207-214, 2002.
Railsback, L. B., Gibbard, P. L., Head, M. J., Voarintsoa, N. R. G., and Toucanne, S.: An optimized scheme of lettered marine isotope substages for the last 1.0 million years, and the climatostratigraphic nature of isotope stages and substages, Quaternary Science Reviews, 111, 94-106, 2015.
Ritz, C., Rommelaere, V., and Dumas, C.: Modeling the evolution of Antarctic ice sheet over the last 420,000 years: Implications for altitude changes in the Vostok region, Journal of Geophysical Research: Atmospheres, 106, 31943-31964, 2001.
Robinson, A., Calov, R., and Ganopolski, A.: An efficient regional energy-moisture balance model for simulation of the Greenland Ice Sheet response to climate change, 2010.
Roe, G. H., and Lindzen, R. S.: The mutual interaction between continental-scale ice sheets and atmospheric stationary waves, Journal of Climate, 14, 1450-1465, 2001.
Saito, F., and Abe-Ouchi, A.: Thermal structure of Dome Fuji and east Dronning Maud Land, Antarctica, simulated by a three-dimensional ice-sheet model, Annals of Glaciology, 39, 433-438, 2004.
Schilt, A., Baumgartner, M., Blunier, T., Schwander, J., Spahni, R., Fischer, H., and Stocker, T. F.: Glacial--interglacial and millennial-scale variations in the atmospheric nitrous oxide concentration during the last 800,000 years, Quaternary Science Reviews, 29, 182-192, 2010.
Schloesser, F., Friedrich, T., Timmermann, A., DeConto, R. M., and Pollard, D.: Antarctic iceberg impacts on future Southern Hemisphere climate, Nature Climate Change, 9, 672-677, 2019.
Schoof, C.: Ice sheet grounding line dynamics: Steady states, stability, and hysteresis, Journal of Geophysical Research: Earth Surface, 112, 2007.

https://doi.org/10.5194/cp-2020-46
Preprint. Discussion started: 27 March 2020

Spratt, R. M., and Lisiecki, L. E.: A Late Pleistocene sea level stack, Climate of the Past, 12, 1079-1092, 2016.
Stap, L. B., Van de Wal, R. S. W., De Boer, B., Bintanja, R., and Lourens, L. J.: Interaction of ice sheets and climate during the past 800 000 years, Climate of the Past, 10, 2135-2152, 2014.
Stein, K., Timmermann, A., Kwon, E. Y., and Friedrich, T.: Timing and magnitude of Southern Ocean sea ice/carbon cycle feedbacks, Proceedings of the National Academy of Sciences, 2020.
Svendsen, J. I., Alexanderson, H., Astakhov, V. I., Demidov, I., Dowdeswell, J. A., Funder, S., Gataullin, V., Henriksen, M., Hjort, C., and Houmark-Nielsen, M.: Late Quaternary ice sheet history of northern Eurasia, Quaternary Science Reviews, 23, 1229-1271, 2004.
Tigchelaar, M., Timmermann, A., Pollard, D., Friedrich, T., and Heinemann, M.: Local insolation changes enhance Antarctic interglacials: Insights from an 800,000-year ice sheet simulation with transient climate forcing, Earth and Planetary Science Letters, 495, 69-78, 10.1016/j.epsl.2018.05.004, 2018.
Timm, O., and Timmermann, A.: Simulation of the last 21 000 years using accelerated transient boundary conditions, Journal of Climate, 20, 4377-4401, 2007.
Timmermann, A., Knies, J., Timm, O. E., Abe-Ouchi, A., and Friedrich, T.: Promotion of glacial ice sheet buildup 60–115 kyr BP by precessionally paced Northern Hemispheric meltwater pulses, Paleoceanography, 25, 2010.
Timmermann, A., Sachs, J., and Timm, O. E.: Assessing divergent SST behavior during the last 21 ka derived from alkenones andG. ruber-Mg/Ca in the equatorial Pacific, Paleoceanography, 29, 680-696, 2014.
Timmermann, A., and Friedrich, T.: Late Pleistocene climate drivers of early human migration, Nature, 538, 92-95, 10.1038/nature19365, 2016.
Uppala, S. M., Kållberg, P., Simmons, A., Andrae, U., Bechtold, V. D. C., Fiorino, M., Gibson, J., Haseler, J., Hernandez, A., and Kelly, G.: The ERA-40 re-analysis, Quarterly Journal of the Royal Meteorological Society: A journal of the atmospheric sciences, applied meteorology and physical oceanography, 131, 2961-3012, 2005.
Van Den Berg, J., van de Wal, R., and Oerlemans, H.: A mass balance model for the Eurasian Ice Sheet for the last 120,000 years, Global and Planetary Change, 61, 194-208, 2008.
Vizcaino, M., Mikolajewicz, U., Ziemen, F., Rodehacke, C. B., Greve, R., and Van Den Broeke, M. R.: Coupled simulations of Greenland Ice Sheet and climate change up to AD 2300, Geophysical Research Letters, 42, 3927-3935, 2015.
Waelbroeck, C., Labeyrie, L., Michel, E., Duplessy, J. C., McManus, J. F., Lambeck, K., Balbon, E., and Labracherie, M.: Sea-level and deep water temperature changes derived from benthic foraminifera isotopic records, Quaternary Science Reviews, 21, 295-305, 2002.
Weertman, J.: Stability of ice-age ice sheets, Journal of Geophysical Research, 66, 3783-3792, 1961.
Willeit, M., Ganopolski, A., Calov, R., and Brovkin, V.: Mid-Pleistocene transition in glacial cycles explained by declining CO_2 and regolith removal, Science Advances, 5, eaav7337, 2019.
Yamagishi, T., Abe-Ouchi, A., Saito, F., Segawa, T., and Nishimura, T.: Re-evaluation of paleo-accumulation parameterization over Northern Hemisphere ice sheets during the ice age examined with a high-resolution AGCM and a 3-D ice-sheet model, Annals of Glaciology, 42, 433-440, 2005.
Yin, Q. Z., and Berger, A.: Individual contribution of insolation and CO_2 to the interglacial climates of the past 800,000 years, Climate Dynamics, 38, 709-724, 2012.
Yoshimori, M., Reader, M., Weaver, A., and McFarlane, N.: On the causes of glacial inception at 116 kaBP, Climate Dynamics, 18, 383-402, 2002.
Ziemen, F., Kapsch, M.-L., Klockmann, M., and Mikolajewicz, U.: Heinrich events show two-stage climate response in transient glacial simulations, Climate of the Past, 15, 153-168, 2019.

https://doi.org/10.5194/cp-2020-46
Preprint. Discussion started: 27 March 2020

Climate of the Past Discussions
Open Access
EGU

Experiment Number	Orbitally Forced	GHG Forced	N_A	α	m (Wm^{-2})
1 **(BLS)**	**Y**	**Y**	**5**	**2**	**125**
2	**N**	**N**	5	2	125
3	Y	**N**	5	2	125
4	**N**	Y	5	2	125
5	Y	Y	5	2	125
6	Y	Y	5	**1.8**	125
7	Y	Y	5	**2.2**	125
8	Y	Y	5	**2.5**	125
9	Y	Y	5	**3**	125
10	Y	Y	5	2	**80**
11	Y	Y	5	2	**100**
12	Y	Y	5	2	**120**
13	Y	Y	5	2	**130**
14	Y	Y	5	2	**140**
15	Y	Y	5	2	**150**

Table 1: List of all experiments. Values in bold represent the difference from the baseline simulation (BLS, experiment number 1). N_A represents the PSUIM vs LOVECLIM acceleration factor (Sect 2.3). α represents the GHG sensitivity scaling factor (Sect. 2.1) and m represents the constant parameter in the surface energy balance equation (Equation 1, Sect. 2.2). All experiments are run at $1 \times 0.5°$ resolution for the Northern Hemisphere and 40×40 km polar stereographic resolution for Antarctica.

https://doi.org/10.5194/cp-2020-46
Preprint. Discussion started: 27 March 2020

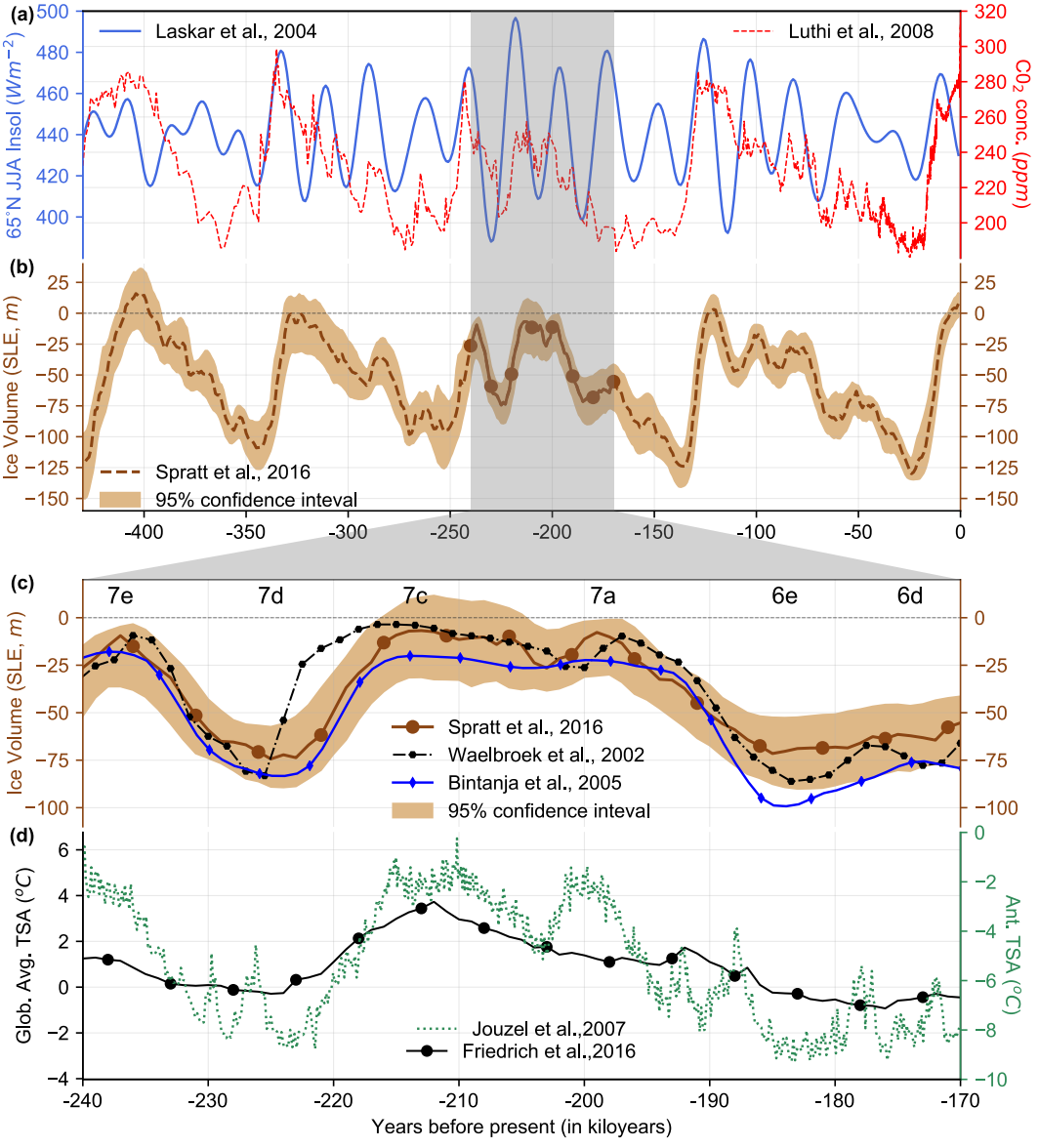

615

Figure 1: Overview of the forcings and reconstructions relevant to this study. From top to bottom: (a) summer insolation at 65°N (Wm^{-2}, blue (Laskar et al., 2004)) and CO_2 concentration (ppm, red (Lüthi et al., 2008)) over the last 430ka; (b) Sea level reconstructions (m) along with 95% confidence limits from Spratt and Lisiecki (2016) (brown) since the Mid Brunhes event. Notice
620 **the relatively cold MIS 7; (c) Sea level reconstructions (m) from Spratt and Lisiecki (2016) (brown), Waelbroeck et al. (2002) (black) and Bintanja et al. (2005) (blue) over MIS 7 (240-170ka); (d) Global average surface air temperature anomaly reconstructed from proxies (°C, black (Friedrich et al., 2016)) and Antarctic temperature anomaly relative to present day (°C, green (Jouzel et al., 2007)). The lettering convention of MIS substages as suggested by Railsback et al. (2015).**

https://doi.org/10.5194/cp-2020-46
Preprint. Discussion started: 27 March 2020

Climate of the Past Discussions
Open Access
EGU

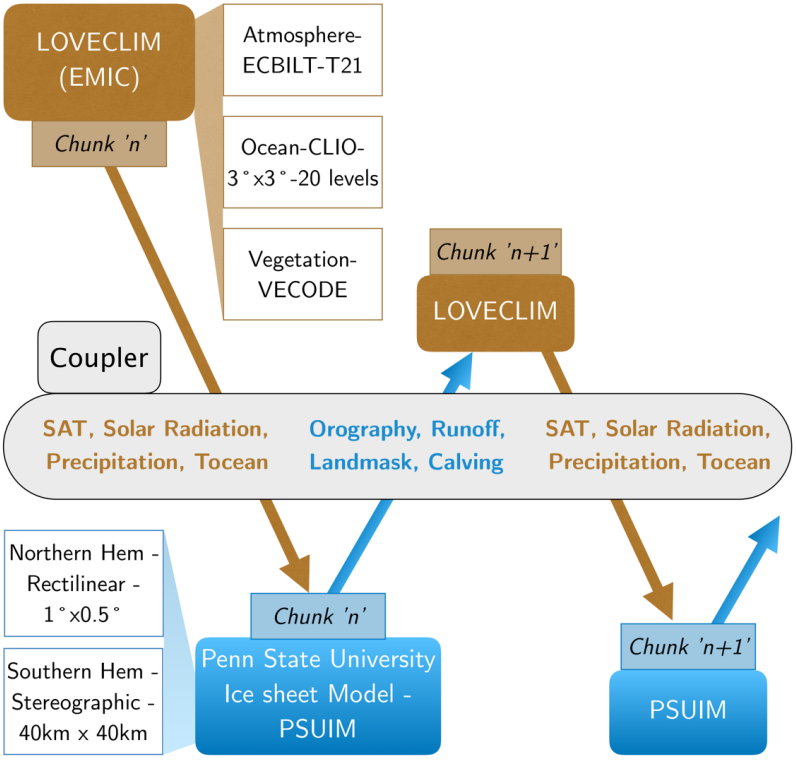

625

Figure 2: Schematic of the coupling between LOVECLIM and PSUIM. SAT is the surface air temperature and Tocean is the ocean temperature at a depth of 400m. Refer to Sect. 2.3 for details.

https://doi.org/10.5194/cp-2020-46
Preprint. Discussion started: 27 March 2020

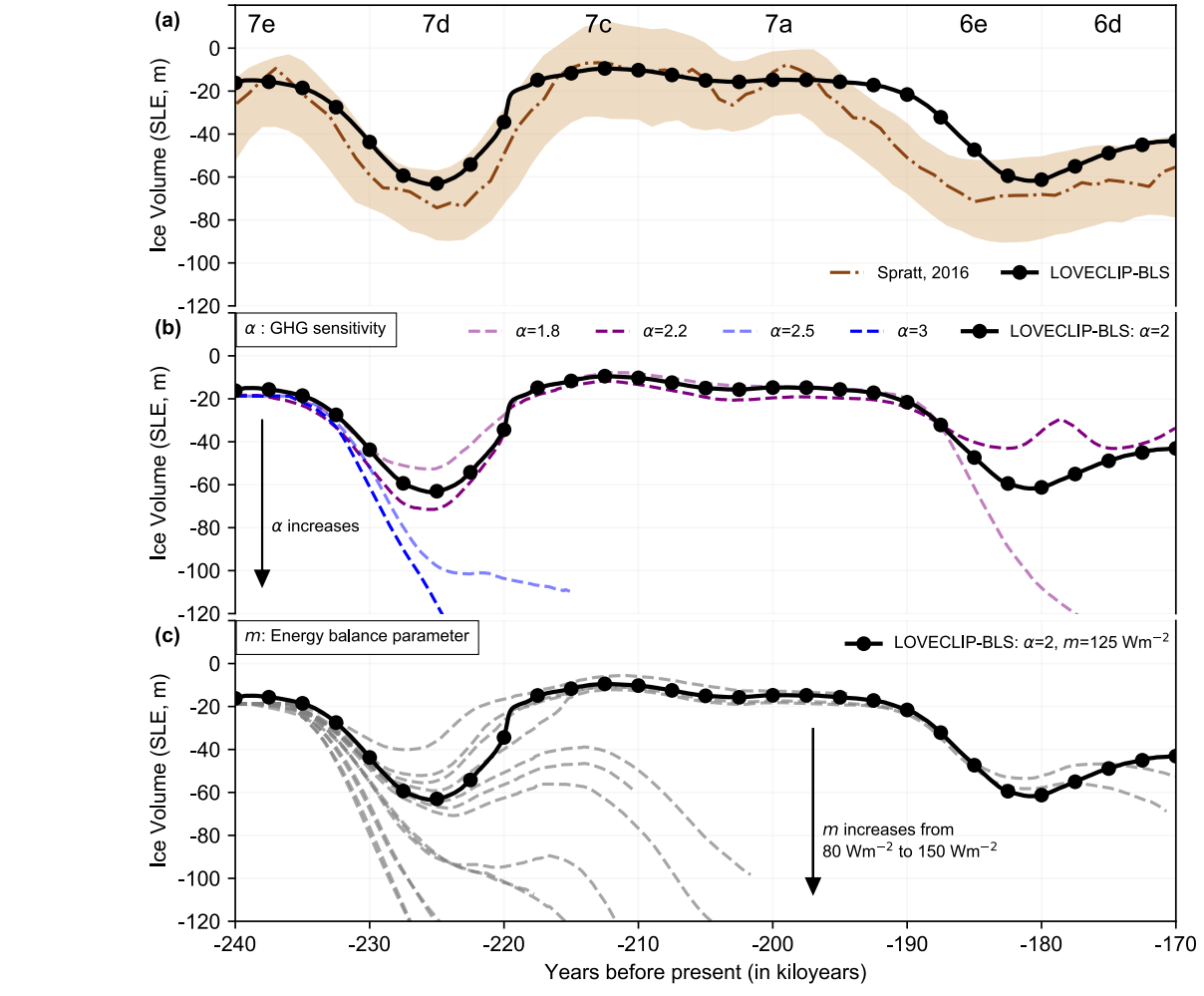

630 **Figure 3: Transient simulation and parameter sensitivity over MIS 7. (a) Sea level reconstruction (m) of Spratt and Lisiecki (2016) (brown) and total ice volume (in terms of SLE, m) from LOVECLIP baseline simulation (BLS, Experiment 1 in Table 1 using α=2 and m=125 Wm^{-2}). (b) LOVECLIP ensembles with varying GHG sensitivities (α) and m of 125 Wm^{-2}. The best results are obtained for an α of 2. (c) LOVECLIP ensembles with α of 2 and different values of the energy balance parameter (m, Wm^{-2}). The best results are obtained for an m of 125 Wm^{-2} (BLS).**

635

https://doi.org/10.5194/cp-2020-46
Preprint. Discussion started: 27 March 2020

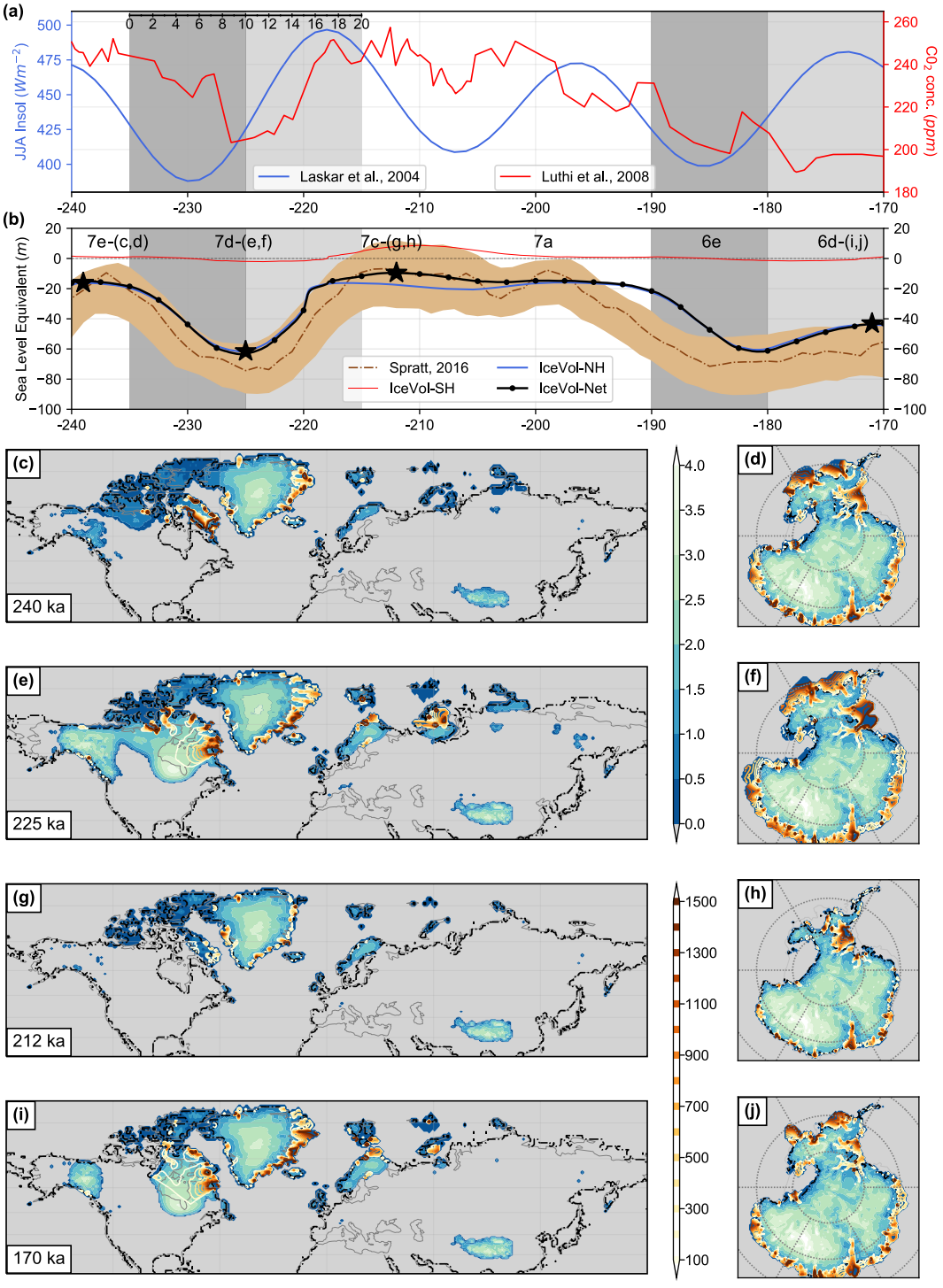

Figure 4: Maps of ice height and ice velocity from our transient coupled climate-ice sheet simulation over MIS 7. (a) JJA mean insolation at 65°N (Wm^{-2}, blue, *(Laskar et al., 2004)*) and CO_2 concentration (ppm, red *(Lüthi et al., 2008)*). The dark grey and light grey patches in the backgrounds of (a) and (b) refer to two 20ky periods leading into a glacial inception (10ky) and immediately after a glacial inception (10ky). The duration of these periods (20ky) is marked by a small scale on the top left and used in Figure 6. (b) Global sea level estimates (m) from *Spratt and Lisiecki (2016)* (brown) and sea level equivalent of ice volume from SH (red), NH

https://doi.org/10.5194/cp-2020-46
Preprint. Discussion started: 27 March 2020

Climate of the Past Discussions
Open Access
EGU

(blue) and total (black) from our transient simulation. The marked stars on the simulated SLE represent four instances corresponding to MIS 7e (240ka), MIS 7d (225ka), MIS 7c (212ka) and MIS 6 (170ka). (c) Ice thickness (solid colors, km); basal ice velocity (colored contours, my^{-1}) and the grounding line (thick black lines) for the Northern Hemisphere at 240ka, initial condition. (d) Same as (c) but for the southern hemisphere. (e) & (f) Same as (c) and (d), but for 225 ka. (g) & (h) Same as (c) and (d), but for 212 ka. (i) & (j) Same as (c) and (d), but for 170 ka.

https://doi.org/10.5194/cp-2020-46
Preprint. Discussion started: 27 March 2020

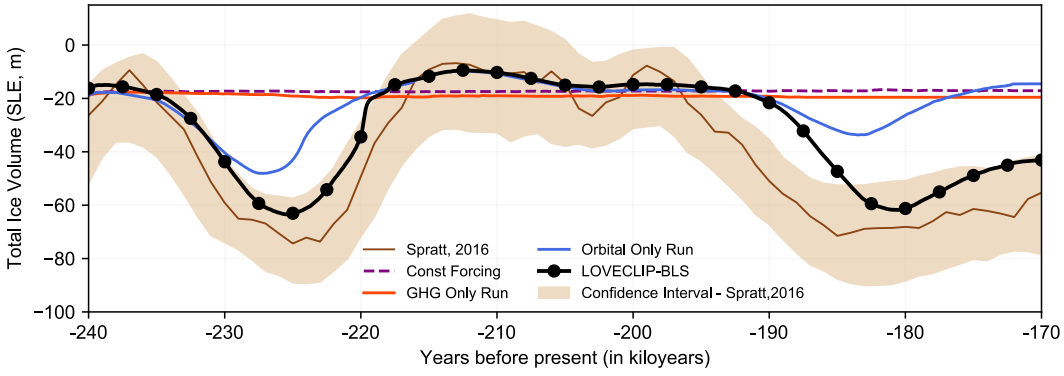

650 **Figure 5: Effects of orbital and GHG forcings on simulated ice volumes during MIS 7. Sea level reconstruction (m) and 95% confidence interval of Spratt and Lisiecki (2016) (brown). Total ice volume (in terms of SLE, m) from transient LOVECLIP simulations with: (i) constant orbital and GHG values set at 240ka (dashed purple line); (ii) orbital values set at 240ka but time varying GHG values (red); (iii) time varying orbital values with GHG values set at 240ka (blue); and (iv) time varying orbital and GHG values (black marked, BLS). All experiments are conducted with an α value of 2 and *m* of 125 Wm^{-2}.**

https://doi.org/10.5194/cp-2020-46
Preprint. Discussion started: 27 March 2020

Climate of the Past
Discussions
Open Access
EGU

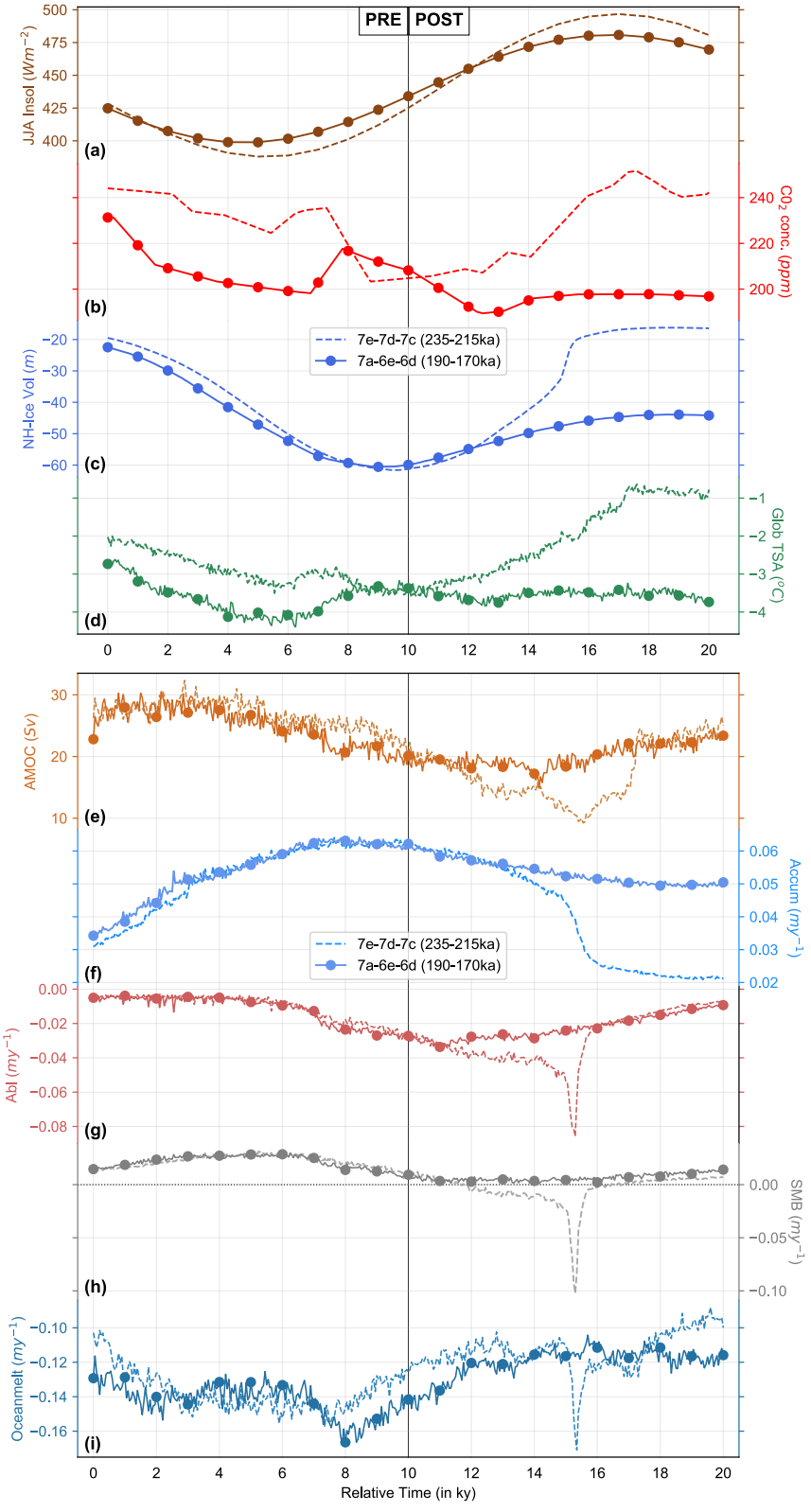

655

https://doi.org/10.5194/cp-2020-46
Preprint. Discussion started: 27 March 2020

Climate of the Past Discussions
Open Access
EGU

Figure 6: Comparison between two glacial inception scenarios. Different variables over two 20k year periods (relative time) during pre-inception (left half) and post inception (right half) over the Northern Hemisphere are plotted. Variables from the earlier period (235-215ka) are plotted in dashed lines while that of the later period (190-170ka) are plotted in circled solid lines. (a) JJA mean insolation at 65°N (Wm^{-2}, *(Laskar et al., 2004)*). (b) CO_2 concentration (ppm, *(Lüthi et al., 2008)*). (c) Simulated Northern Hemisphere ice volume, in sea level equivalents (m). (d) Global average surface temperature anomaly (°C). (e) Temporal evolution of AMOC (Sv). (f) Average accumulation rate over Northern Hemisphere ice (my^{-1}). (g) Average surface melt rate over Northern Hemisphere ice (my^{-1}). (h) Net surface mass balance over the Northern Hemisphere ice (my^{-1}). (i) Average subshelf melt rate over Northern Hemisphere (my^{-1}).

https://doi.org/10.5194/cp-2020-46
Preprint. Discussion started: 27 March 2020

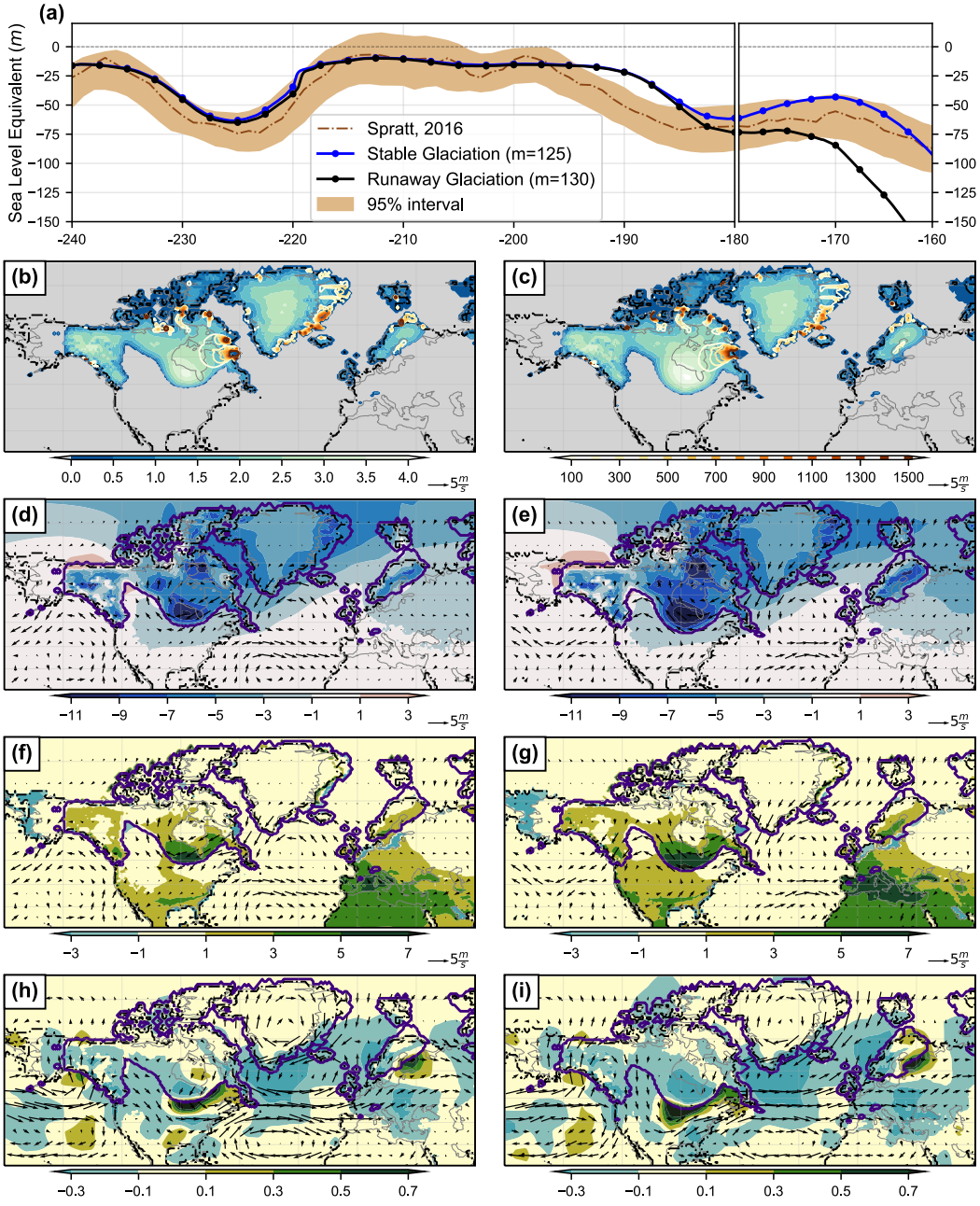

Figure 7: Bifurcation of the system at 180ka while transitioning into MIS 6 over Laurentide. (a) Sea level reconstruction (m) and 95% confidence interval of Spratt and Lisiecki (2016) (brown). Total ice volume (in terms of SLE, m) from two ensembles of LOVECLIP, one that leads to a stable glacial inception (blue; α=2, m=125 Wm^{-2}) and another into a runaway glaciation (black; α=2, m=130 Wm^{-2}). Climate and ice sheet variables at 180ka from the stable glaciation on the left column (b, d, f and h) and runaway glaciation on the right (c, e, g and i). (b,c) Ice thickness (solid colors, km) overlaid with basal ice velocity (colored contours, my^{-1}) and the grounding line (black dotted lines). (d,e) Surface temperature anomalies ($^{\circ}C$) overlaid with *anomalous* wind vectors at 800hPa (ms^{-1}). (f,g) Net mass balance anomalies (my^{-1}) overlaid with *anomalous* winds (ms^{-1}). (h,i) Rainfall anomalies (my^{-1}) overlaid with *absolute* winds (ms^{-1}). The purple contours in (d) to (i) mark the boundaries of the ice sheets. Anomalies here are with respect to the initial condition at 240ka. Anomalies over the Eurasian and Siberian ice sheets are small and not shown.